

Common Glass-Forming Spin-Liquid State in the Pyrochlore Magnets $\text{Dy}_2\text{Ti}_2\text{O}_7$ and $\text{Ho}_2\text{Ti}_2\text{O}_7$

Azar B. Eyvazov¹, Ritika Dusad¹, Timothy J. S. Munsie^{2,3}, Hanna A. Dabkowska², Graeme M. Luke^{2,3,4}, Ethan R. Kassner^{1,5}, J.C. Séamus Davis^{1,6,7,8} and Anna Eyal^{1†}

1. *LASSP, Department of Physics, Cornell University, Ithaca, NY 14853, USA.*
2. *Brockhouse Inst. for Materials Research, McMaster University, Hamilton, ON, Canada.*
3. *Department of Physics, McMaster University, Hamilton, Ontario, L8S 4M1, Canada.*
4. *Canadian Institute for Advanced Research, Toronto, Ontario, M5G 1Z8, Canada.*
5. *Current address: Honeywell International Inc., Golden Valley, MN 55422, USA.*
6. *CMPMS Department, Brookhaven National Laboratory, Upton, NY 11973, USA.*
7. *School of Physics, University of St. Andrews, St. Andrews, Fife KY16 9SS, Scotland.*
8. *Tyndall National Institute, University College Cork, Cork T12R5C, Ireland.*

†. *Correspondence to anna.eyal@gmail.com.*

Despite a well-ordered pyrochlore crystal structure and strong magnetic interactions between the Dy^{3+} or Ho^{3+} ions, no long range magnetic order has been detected in the pyrochlore titanates $\text{Ho}_2\text{Ti}_2\text{O}_7$ and $\text{Dy}_2\text{Ti}_2\text{O}_7$. To explore the actual magnetic phase formed by cooling these materials, we measure their magnetization dynamics using toroidal, boundary-free magnetization transport techniques. We find that the dynamical magnetic susceptibility of both compounds has the same distinctive phenomenology, that is indistinguishable in form from that of the dielectric permittivity of dipolar glass-forming liquids. Moreover, $\text{Ho}_2\text{Ti}_2\text{O}_7$ and $\text{Dy}_2\text{Ti}_2\text{O}_7$ both exhibit microscopic magnetic relaxation times that increase along the super-Arrhenius trajectories analogous to those observed in glass-forming dipolar liquids. Thus, upon cooling below about 2K, $\text{Dy}_2\text{Ti}_2\text{O}_7$ and $\text{Ho}_2\text{Ti}_2\text{O}_7$ both appear to enter the same magnetic state exhibiting the characteristics of a glass-forming spin-liquid.

In the pyrochlore lanthanide-oxides with chemical formula $A_2B_2O_7$, the magnetic rare earth A ions are located at corner sharing tetrahedral sites as shown in Fig. 1a (1). These materials support a multitude of exotic magnetic states (2,3,4), such as spin-ice (5,6), spin-slush (7), and various candidates for quantum spin-liquids (8). $Dy_2Ti_2O_7$ and $Ho_2Ti_2O_7$ have attracted much interest since the discovery of an entropy deficit in both compounds (5,9) along with a similarity to the thermodynamic properties of water ice. In both $Dy_2Ti_2O_7$ and $Ho_2Ti_2O_7$ the large rare-earth magnetic moments of $\mu \sim 10\mu_B$ (10), at the corners of the corner sharing tetrahedral structure, are subject to strong crystal field interactions (11,12), so that in the single-ion ground state spins are only allowed to point towards (away) from the centers of the tetrahedra that share it (see Fig. 1a) (5). Under these circumstances, long-range magnetic dipolar interactions are significant when compared to the nearest-neighbor magnetic exchange coupling. The resulting interaction favors a state in which for each tetrahedron two spins point in and two out, that, by analogy to water ice, was dubbed “spin-ice” (13). One might expect such a constraint to result in an ordered magnetic state that is unique (14), but no such states have ever been observed in these two materials at zero magnetic field (15).

For both $Ho_2Ti_2O_7$ and $Dy_2Ti_2O_7$ the strength of the nearest neighbor dipolar interaction is $D_{nn} \approx 2.35K$, while the nearest neighbor exchange interactions are $J_{nn} \approx -0.52K$ for $Ho_2Ti_2O_7$ and $J_{nn} \approx -1.24K$ for $Dy_2Ti_2O_7$ (16,17). Raman spectroscopy reveals that the phonon spectrum of these two materials differ only slightly and that the crystal field parameters are very similar (18). Dysprosium ions have 7 f-electrons with $J=15/2$ for the single ion angular momenta in the ground state, with the crystal field levels all Kramers doublets; holmium ions, on the other hand, have 8 f-electrons with an integer $J=8$, so its crystal field spectrum has both singlet and doublet energy levels (19). The magnetic heat capacity of both materials has a broad peak at low temperatures (1.2K for $Dy_2Ti_2O_7$ and 1.9K for $Ho_2Ti_2O_7$) (5,9,20). However, $Ho_2Ti_2O_7$ has another peak in heat capacity at much lower temperatures, which is believed to be due to its active nuclear magnetism (20,21). Interpreting the magnetization dynamics of these two systems has proven challenging. Nearest neighbor spin-ice-based models for spin dynamics predict inelastic neutron scattering intensity patterns where “pinch points” are significantly smeared out

compared to the experiments (22,23), and exchange interactions up to third nearest neighbor must be included in the models to replicate the full complexity of these neutron scattering results (24). Models for the magnetic susceptibility $\chi(\omega, T)$ based on dipolar-spin-ice (25), or on the dynamics of a dilute gas of mobile monopoles (4) representing transitions from two-in-two-out to three-in-one-out configurations (26,27) (see Fig. 1b), show significant deviations from the experimental data (25). Moreover, predictions for the temperature dependence of microscopic magnetic relaxation times τ considerably underestimate the divergence of τ at low temperatures (28). Finally, in the absence of magnetic fields, no magnetic order has been detected in either compound (14). Thus, a definitive understanding of the low temperature magnetic state of these materials is lacking.

A recent proposal (29) that the magnetic state of $\text{Dy}_2\text{Ti}_2\text{O}_7$ is the magnetic analog of the diverging viscosity state found in glass-forming dipolar liquids (30,31,32,33) provides a different perspective. Classical glass-forming liquids exhibit universally a super-Arrhenius divergence of microscopic dipolar relaxation times $\tau_0(T)$ of the Vogel-Tamman-Fulcher (VTF) form $\tau_0(T) = A \exp\left(\frac{DT_0}{T-T_0}\right)$ (34), a dielectric function $\varepsilon(\omega, T)$ of the Havriliak-Negami (HN) form $\varepsilon(\omega, T) = \varepsilon_\infty + \frac{\varepsilon_0}{(1+(i\omega\tau_{HN})^\alpha)^\gamma}$ (35,36), and a related time-domain relaxation described by the Kohlrausch-Williams-Watts (KWW) form (37) $\varepsilon(t) = \varepsilon_0 \exp\left[-\left(\frac{t}{\tau_{KWW}}\right)^\beta\right]$. Observation of this combined VTF/HN/KWW phenomenology provides a strong clear identifier of a supercooled glass-forming dipolar fluid (30,31,32,33). $\text{Dy}_2\text{Ti}_2\text{O}_7$ was found to exhibit a precise HN form for its magnetic susceptibility $\chi(\omega, T)$, a general KWW form for the magnetic relaxation, and diverging microscopic magnetic relaxation rates on a VTF trajectory, implying that it is, by analogy, a glass-forming magnetic liquid (29). Here we explore if magnetic fluids with such a phenomenology could be more general in the lanthanide pyrochlore magnetic materials.

Even if glass-forming spin liquid phenomenology were common to such materials, the microscopic parameters are still likely to be specific to each compound. In glass-

forming dipolar liquids, the measure of the correlated and hierarchically blocked dipole dynamics is called the fragility, D , (38) and it characterizes the degree of spatial heterogeneity. D is an indicator of the spread of microscopic relaxation times over different close-by regions in the liquid. The smaller value of D , the more fragile the liquid and the more spatially heterogeneous its dynamics (33,38). By analogy, a more fragile glass-forming spin-liquid would mean an enhancement of the super-Arrhenius behavior of its magnetic relaxation times upon cooling. Such a situation could be caused by less efficient tunneling between spin configurations, due perhaps to differences in monopole creation energies and hopping rates. For the pyrochlore magnets discussed, the chemical potential for monopole-pair generation is dependent on nearest neighbor coupling, J_{eff} (17), which is 1.1K for $Dy_2Ti_2O_7$ and 1.8K for $Ho_2Ti_2O_7$. Moreover, the rate of tunneling of the monopole excitations depends on the off-diagonal components of the dipolar interactions of neighboring spin (39). The reason for this is the strong Ising-like behavior of the magnetic ions (40), with the energy barriers to the first excited crystal field state being $\Delta \sim 240K$ for $Ho_2Ti_2O_7$ and $\sim 380K$ for $Dy_2Ti_2O_7$ (17). Additionally, the fact that the effective energy scale for spin-flip dynamics is on the order of several J_{eff} rather than Δ implies that spin flips occur by quantum tunneling (39). Since the transverse fields in $Ho_2Ti_2O_7$ are more pronounced than in $Dy_2Ti_2O_7$ resulting in a more effective quantum tunneling at low magnetic fields (19), monopole hopping in $Ho_2Ti_2O_7$ is expected to be more efficient. In that case, one might anticipate a less fragile glass-forming spin-liquid in $Ho_2Ti_2O_7$ as compared to $Dy_2Ti_2O_7$.

Experimental setup

To explore the relationship between the magnetization dynamics of $Ho_2Ti_2O_7$ and $Dy_2Ti_2O_7$ we used a boundary-free arrangement to measure the AC susceptibility and time dependent magnetization relaxation characteristics of the two materials at $T \leq 2$ K. For the boundary-free magnetization measurements, holes were drilled carefully through the center of disk shaped samples of $Ho_2Ti_2O_7$ and $Dy_2Ti_2O_7$ single crystals. A superconducting toroidal solenoid (STS) was then made by winding fine NbTi wire around the toroidal samples (Fig. 1c,d). Using a toroidal geometry for both the samples and the magnetization sensors means that the superconducting toroidal solenoid can be used to both drive

magnetization flow azimuthally and to simultaneously and directly determine $d\mathbf{M}/dt$ throughout. More importantly, it removes any boundaries in the direction of the magnetization transport (Fig. 1c). The coil EMF due to changes in both the applied azimuthal field $\mathbf{H}(t)$ and sample magnetization $\mathbf{M}(t)$ is given by

$$\mathbf{V}_{total}(t, T) = -\mu_0 N A \left(\frac{d\mathbf{H}}{dt} + \frac{d\mathbf{M}}{dt} \right) \quad (1)$$

where N is the number of turns in the solenoid and A is the effective cross-sectional area of the solenoid. Thus, the EMF due to magnetization dynamics in the sample is

$$\mathbf{V}(t, T) = -\mu_0 N A \frac{d\mathbf{M}(t, T)}{dt} \quad (2)$$

For an applied AC field $\mathbf{H} = \mathbf{H}_0 \exp(i\omega t)$ we expect that $\mathbf{M} = \mathbf{M}(\omega) \exp(i\omega t)$ with some complex amplitude $\mathbf{M}(\omega)$, so that

$$V(\omega, T) = -i\mu_0 N A \omega M(\omega, T) \quad (3)$$

The definition of the magnetic susceptibility is

$$\mathbf{M}(\omega, T) = \chi(\omega, T) \mathbf{H}(\omega) \quad (4)$$

In a solenoid $H_0 = nI$, where n is the number of turns per unit length, so the EMF is given by

$$V = V_x + iV_y = -i\mu_0 N A \omega \chi(\omega) H_0 = -iI\omega L [\chi'(\omega, T) - i\chi''(\omega, T)] \quad (5)$$

where L is the geometric inductance of the STS pickup coil. Currents of up to 200 mA can be applied to our STS coils, yielding azimuthal applied fields of magnitude up to $|B|=2.5$ mT, or $|H|=2222$ A/m. The AC susceptibility of the compounds measured was determined typically by applying ~ 10 mA currents in a frequency range of 10 Hz – 100 kHz using a 4-probe impedance measurement of the STS. The inductance, L , of the STS was measured at $T=50$ mK, where neither of the materials show any magnetic activity in the frequency range measured, and then used in Eqn. (5) to calculate the susceptibility $\chi(\omega, T)$ data from the voltage readings.

Results

During data acquisition, the voltage over the STS was measured every 20 ms throughout the following excitation protocol: (a) apply magnetic field in a clockwise direction by turning on a current $I=50$ mA in the STS, (b) set field to zero by turning off the current, (c) apply a magnetic field in the counter clockwise direction by turning on a current $I=-50$ mA in the opposite direction and (d) again zero the field. This protocol was repeated 150 times per temperature for each material at each temperature, and the results were averaged to improve data quality and fitting. For both materials, no difference in relaxation characteristics was observed when the magnetic field was turned on or off, as well as when the magnetic field was applied in one azimuthal direction or the opposite. At long times, after the initial sharp change in the field, the EMF that was generated in the STS decayed to zero, indicating that $J=d\mathbf{M}/dt$ (27,29) always decays to zero, despite the fact there are no terminating boundaries in our geometry. Figures 2a,b depict the measured magnetization relaxation characteristics $d\mathbf{M}/dt$ of $\text{Ho}_2\text{Ti}_2\text{O}_7$ and $\text{Dy}_2\text{Ti}_2\text{O}_7$ respectively in the temperature range 0.6 K-0.95 K. The plots show the measured voltage induced across the STS, by the magnetization dynamics of the sample versus time after the application of a DC field. These data sets at each temperature were fitted by a KWW type stretched exponential decay $V(t) = V_0 \exp(-(t/\tau)^\beta)$, with several representative fits shown in Fig 2a,b as fine colored curves. Although a simple exponential decay cannot fit any of these data at any temperature, the KWW form provides an excellent fit for all. The insets of Fig. 3a and b show how the stretching parameter, β , is different from unity over the temperature range of the DC measurements for both compounds. More importantly, Figs 3a,b reveal the universal applicability of the KWW form of both samples for the whole temperature range. Here, the normalized EMF $V(t)/V_0$ is plotted against the modified time parameter $x = (t/\tau)^\beta$ for each temperature, with the result that all the magnetization transient data from both materials collapses onto a single line with unit slope. This remarkable agreement of magnetization decay dynamics of both $\text{Ho}_2\text{Ti}_2\text{O}_7$ and $\text{Dy}_2\text{Ti}_2\text{O}_7$ with a KWW form implies that both these systems are in the same state, a glass-forming spin-liquid.

The AC magnetic susceptibility of the toroidal samples of $\text{Ho}_2\text{Ti}_2\text{O}_7$ and $\text{Dy}_2\text{Ti}_2\text{O}_7$ was measured in the temperature range 0.9 K-2 K. For the compounds in this paper, we observed that below 0.5 K the EMF generated in the STS showed virtually no temperature dependence down to 50 mK, the lowest temperature at which AC measurements were attempted. The AC voltage measured at the lowest temperature was subtracted from the measurement at the temperatures of interest to deduce the susceptibility $\chi(\omega, T) = \chi'(\omega, T) - i\chi''(\omega, T)$. Figs. 2c and 2d present the measured real (χ') and imaginary (χ'') parts of the susceptibilities for the samples measured versus frequency, in the range 10- 10^5 Hz for $\text{Ho}_2\text{Ti}_2\text{O}_7$ and 10- 10^4 Hz for $\text{Dy}_2\text{Ti}_2\text{O}_7$. The data sets taken at different temperatures are labeled by a color/symbol code as indicated.

Models of AC susceptibility that assume a single relaxation time of the Debye form $\chi' - i\chi'' = \frac{\chi_0}{[1 + (i\omega\tau)]}$, for example those of free monopole motion (26), are not compatible with the measured $\chi(\omega, T)$ for either $\text{Ho}_2\text{Ti}_2\text{O}_7$ and $\text{Dy}_2\text{Ti}_2\text{O}_7$ at any frequency or temperature within these ranges. By contrast, a Havriliak-Negami form modifies the simple Debye susceptibility with two exponents, α and γ , and corresponds to a system where there is a distribution of relaxation times

$$\chi' - i\chi'' = \frac{\chi_0}{[1 + (i\omega\tau)^\alpha]^\gamma} + \chi_\infty \quad (6)$$

Figs. 2c and 2d depict our measured data for both $\text{Ho}_2\text{Ti}_2\text{O}_7$ and $\text{Dy}_2\text{Ti}_2\text{O}_7$ respectively. The top panels showing the real part of the measured magnetic susceptibility versus frequency, as calculated from our measured voltage, using equation (5), and the bottom panels presenting the imaginary part of the susceptibility versus frequency. The different colors show data from different temperatures in the range 0.9K to 2K. For $\text{Dy}_2\text{Ti}_2\text{O}_7$, both exponents of the HN fit deviate from unity for the majority of the temperature range (inset of Fig. 3d). Overall, the susceptibility for both materials shows a very good global agreement with the HN form for all temperatures and frequencies measured, as demonstrated for unprocessed $\chi(\omega, T)$ by the fine black fit lines shown for every temperature in Figs 2c,d. Figures 3c and 3d show the collapse of all these dynamical susceptibility $\chi(\omega, T)$ data for all temperatures and both materials onto the single HN

form (29) as indicated by the fine solid curves. The horizontal axis in the figure is the frequency, scaled by the HN parameters, and the vertical axes are the real and imaginary parts of the scaled HN susceptibility $G(\gamma, \chi_0, \chi)$ (a full mathematical derivation can be found in Ref. 29). The scaling parameters, which are the fit parameters of the HN form for each temperature, are plotted in the insets of the figure. The quality of fits, while comprehensively good versus ω and T for both materials (Fig. 2c,d), is obviously slightly different between $\text{Ho}_2\text{Ti}_2\text{O}_7$ and $\text{Dy}_2\text{Ti}_2\text{O}_7$ (Fig. 3c,d). This may not be surprising since the frequency range of $\text{Ho}_2\text{Ti}_2\text{O}_7$ experiments is at least two orders of magnitude wider than that for $\text{Dy}_2\text{Ti}_2\text{O}_7$. In any case, this observation of a universal Havriliak-Negami form for all the $\chi(\omega, T)$ susceptibility data (Fig. 3c,d) constitutes a second robust indication that both these materials are homologous glass-forming spin-liquids.

Finally, to explore the microscopic magnetic relaxation dynamics of these systems, we need a form to relate the relaxation times obtained from the time-domain measurements to those from the frequency-domain. Numerical studies have linked the exponents and relaxation time parameters of the two forms (41), which can be used for a unified analysis of our data. Using the values in Table I of Ref. (41) we can generate values for $\ln \frac{\tau_{HN}}{\tau_{KWW}}$, enabling a conversion of the relaxation times from the time-domain measurements to the frequency-domain. Figure 4a depicts the combined time- and frequency-domain relaxation-time data for $\text{Ho}_2\text{Ti}_2\text{O}_7$ ($T \geq 0.8$ K) and $\text{Dy}_2\text{Ti}_2\text{O}_7$ respectively (the relaxation-times obtained from the time-domain measurement, τ_{KWW} , were converted to τ_{HN} by the procedure described above) with the horizontal axis being the inverse temperature. Obviously, the relaxation-time data for both materials diverge on a trajectory that is faster than Arrhenius, which would produce a straight line in Fig. 4a. Indeed, many groups have previously reported relaxation-time data showing the general behavior of a divergence that is faster than Arrhenius (28,42,43,44), and in particular $\text{Ho}_2\text{Ti}_2\text{O}_7$ showing a stronger divergence.

However, when the temperature dependence of the relaxation-time is fit to a VTF form, $\tau(T) = A \exp\left(\frac{DT_0}{T-T_0}\right)$, as shown in Fig. 4b, our findings indicate that both $\text{Dy}_2\text{Ti}_2\text{O}_7$ and $\text{Ho}_2\text{Ti}_2\text{O}_7$ exhibit the non-Arrhenius slowing characteristic of glass-forming liquids.

This form yields $A=1.54 \cdot 10^{-9} \pm 1.47 \cdot 10^{-9}$ s, a fragility parameter $D=62.4 \pm 33.1$ and a VTF temperature $T_0=190.9 \pm 17.5$ mK for $\text{Ho}_2\text{Ti}_2\text{O}_7$, and $A=1.63 \cdot 10^{-4} \pm 1.58 \cdot 10^{-5}$ s, $D=13.1 \pm 1.1$ and $T_0=256.8 \pm 12.2$ mK for $\text{Dy}_2\text{Ti}_2\text{O}_7$. The fragility parameter and the estimated high temperature relaxation-time depend strongly on the materials studied. However, T_0 , the lowest temperature at which both materials may be expected by analogy with dipolar glass-forming fluids to enter a magnetic glass phase, is much closer in value. Here, once again, we find in the common VTF form for $\tau(T)$, a clear indication that both $\text{Dy}_2\text{Ti}_2\text{O}_7$ and $\text{Ho}_2\text{Ti}_2\text{O}_7$ are glass-forming spin-liquids.

Discussion

Previous comparison studies of AC susceptibility of these two compounds (28,43) identified differences in the spread of microscopic relaxation times. When normalized χ'' versus normalized frequency (at different temperatures) were compared between them, it was noted that the $\log(f_{\text{FWHM}}/f_{\text{max}})$ taken as indicating the broadness of the absorption spectra, was greater for $\text{Ho}_2\text{Ti}_2\text{O}_7$ than for $\text{Dy}_2\text{Ti}_2\text{O}_7$. Also, as the characteristic relaxation time τ for these compounds was taken to be $\tau=1/2\pi f_{\text{max}}$, where f_{max} was the frequency at which χ'' peaked, an observed additional broadness in normalized χ'' vs frequency indicated greater spread in relaxation times in $\text{Ho}_2\text{Ti}_2\text{O}_7$. Finally, the asymmetry of normalized χ'' vs. normalized frequencies was noted to be greater in $\text{Ho}_2\text{Ti}_2\text{O}_7$ than in $\text{Dy}_2\text{Ti}_2\text{O}_7$ (28). There is good qualitative consistency between those data and the results of our studies show in Figs. 2 and 3. Indeed, when considering the asymmetry parameter in our Havriliak-Negami fits of scaled susceptibility $G(\gamma, \chi_0; \chi)$ vs normalized dimensionless frequency units (Fig. 3c,d), one sees that $\text{Ho}_2\text{Ti}_2\text{O}_7$ measurements are significantly more skewed than $\text{Dy}_2\text{Ti}_2\text{O}_7$. Moreover, the well-known difference in microscopic energy scales between $\text{Ho}_2\text{Ti}_2\text{O}_7$ and $\text{Dy}_2\text{Ti}_2\text{O}_7$, also consistent with our findings in Fig. 4, is a global effect quite unlikely to be due to random disorder or off-stoichiometry. Thus, to capture these observed systematic differences of between the Havriliak-Negami susceptibility of $\text{Ho}_2\text{Ti}_2\text{O}_7$ and $\text{Dy}_2\text{Ti}_2\text{O}_7$ requires a microscopic theory. One such posits a fluid of emergent delocalized magnetic monopoles (4,17) in which flips of the real magnetic dipoles are recast as two opposite magnetic charges that, through a sequence of spin flips, may form a fluid of delocalized magnetic monopoles and anti-

monopoles (4) with transport characteristics controlling the magnetization dynamics (45). Whether this model is consistent with the observed magnetization dynamics phenomenology of $\text{Ho}_2\text{Ti}_2\text{O}_7$ and $\text{Dy}_2\text{Ti}_2\text{O}_7$, including those reported in Refs 28,43 and herein in Figs. 2, 3, and 4, remains to be determined.

To summarize: for purposes of comparison, we measured the AC magnetic susceptibility $\chi(\omega, T)$ and time dependent magnetic relaxation behavior in the low-temperature magnetic states of both $\text{Dy}_2\text{Ti}_2\text{O}_7$ and $\text{Ho}_2\text{Ti}_2\text{O}_7$; we used identical boundary-free sample geometries within a superconducting toroidal solenoid. We find that, for both materials, the DC relaxation follows a stretched exponential, KWW form (Fig. 3a,b), the AC susceptibility follows a HN form (Fig. 3,d). Above 0.8 K, the microscopic relaxation time for both materials diverges along a super-Arrhenius trajectory (Fig. 4b). These phenomena all indicate that the magnetic state of both materials is the magnetic analog of a glass-forming dipolar liquid. The difference in apparent fragility between these glass-forming spin-liquids may be explained if the disorder generated by the magnetization transport in $\text{Dy}_2\text{Ti}_2\text{O}_7$ is enhanced compared to that in $\text{Ho}_2\text{Ti}_2\text{O}_7$ at the same temperature. And, while this general glass-forming spin-liquid phenomenology has now been observed in both $\text{Dy}_2\text{Ti}_2\text{O}_7$ and $\text{Ho}_2\text{Ti}_2\text{O}_7$, it is not yet clear how it can be consistent with theory for spin-ice magnetization dynamics due to the motion of emergent monopoles. However, recent studies using the spin-ice Hamiltonian extended to include stronger next nearest neighbor interactions do report the existence of new forms of dynamical magnetic heterogeneity with extremely slow relaxation times for some spins (7,46). Thus, the type of glass-forming spin-liquid phenomenology that we have discovered for both $\text{Dy}_2\text{Ti}_2\text{O}_7$ and $\text{Ho}_2\text{Ti}_2\text{O}_7$ can exist, at least in principle, in dipolar spin-ice.

Additional Information

Methods

The $\text{Ho}_2\text{Ti}_2\text{O}_7$ and $\text{Dy}_2\text{Ti}_2\text{O}_7$ single crystalline samples studied in this work were synthesized by the G. M. L. group at McMaster university using an optical floating zone furnace. The samples were grown as a boule in O_2 gas under 2 atm pressure [47]. These were subsequently cut into disks of diameter $\sim 6\text{mm}$ and thickness $\sim 1\text{mm}$. (see Fig. 1d). For the boundary-free magnetization measurements, holes of about 2.5 mm diameter were drilled at the center of these disk-shaped samples. A superconducting toroidal solenoid (STS) was then made by winding an 0.09 mm diameter NbTi wire around the sample (see Fig. 1d). Currents of up to 200 mA (fields of up to 2.5 mT) could be applied to the STS coil using low temperature Nb crimp joints. The measurements were performed in a dilution refrigerator, and the signals were measured using lock-in amplifiers.

Data Availability

The relevant data can be supplied to qualified scientists by the authors upon reasonable request.

Competing Financial Interests

The authors declare no competing financial interests.

Acknowledgments

We acknowledge useful and encouraging discussions with S. Bramwell, C. Castelnovo, J. Chalker, H. Changlani, M. Gingras, E.-A. Kim, M.J. Lawler and J. Sethna. J.C.S.D., R.D. and A. E. acknowledge support from the Moore Foundation's EPiQS Initiative through Grant GBMF4544.

Author contributions

A.B.E., R.D and A.E. designed and performed the experiment, analyzed the data and wrote the manuscript; E.R.K. conceived the experimental concept and suggesting a model; T.J.S.M., H.A.D., G.M.L. synthesized the samples used in this study. J.C.S.D. & G.M.L. conceived and supervised the project and wrote the manuscript with key contributions from A.B.E., R.D and A.E.

Figure 1

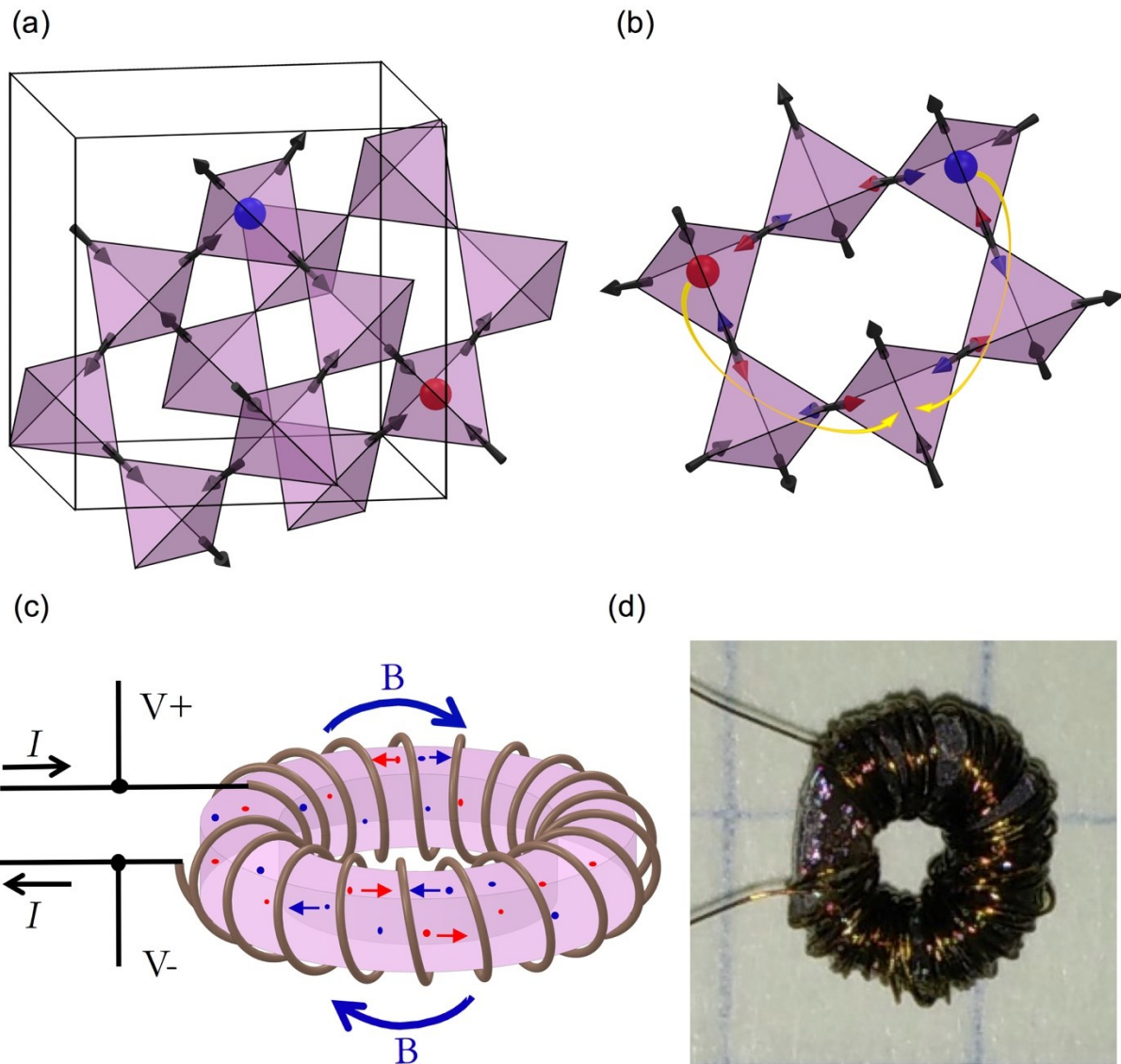


Figure 1

An illustration of the spin-ice sample and our measurement setup.

- (a) Crystal structure of the sublattice of rare earth ions in the pyrochlore titanates. The angular momenta of the ions (Dy^{3+} or Ho^{3+}), at the corners of a network of corner sharing tetrahedra, are constrained to point towards or away from the centers of their surrounding tetrahedra (black arrows). The spin-ice ground state then corresponds to a 2-in 2-out spin configuration for each tetrahedron (as can be seen in a tetrahedron on the left). The excitations from this state are magnetic monopole-like quasi-particles. A 3-in 1-out spin state in a tetrahedron can be represented as a monopole (red ball), and a 3-out 1-in state as an anti-monopole (blue ball).
- (b) These monopoles are highly correlated and can be created, transport (yellow arrows) and then get annihilated on loops of varying sizes. The shortest such loop is shown.
- (c) Measuring the dynamics of magnetization dynamics in a boundary-free environment is done by applying an azimuthal magnetic field in a torus shaped sample. The Superconducting Toroidal Solenoid (STS) used enables us to eliminate the contribution of the demagnetization effect and to allow for accurate measurements both in time and frequency domains.
- (d) A single crystal toroidal sample of $Ho_2Ti_2O_7$ wired with a STS of fine NbTi wire. The outer diameter of the sample is 6mm.

Figure 2

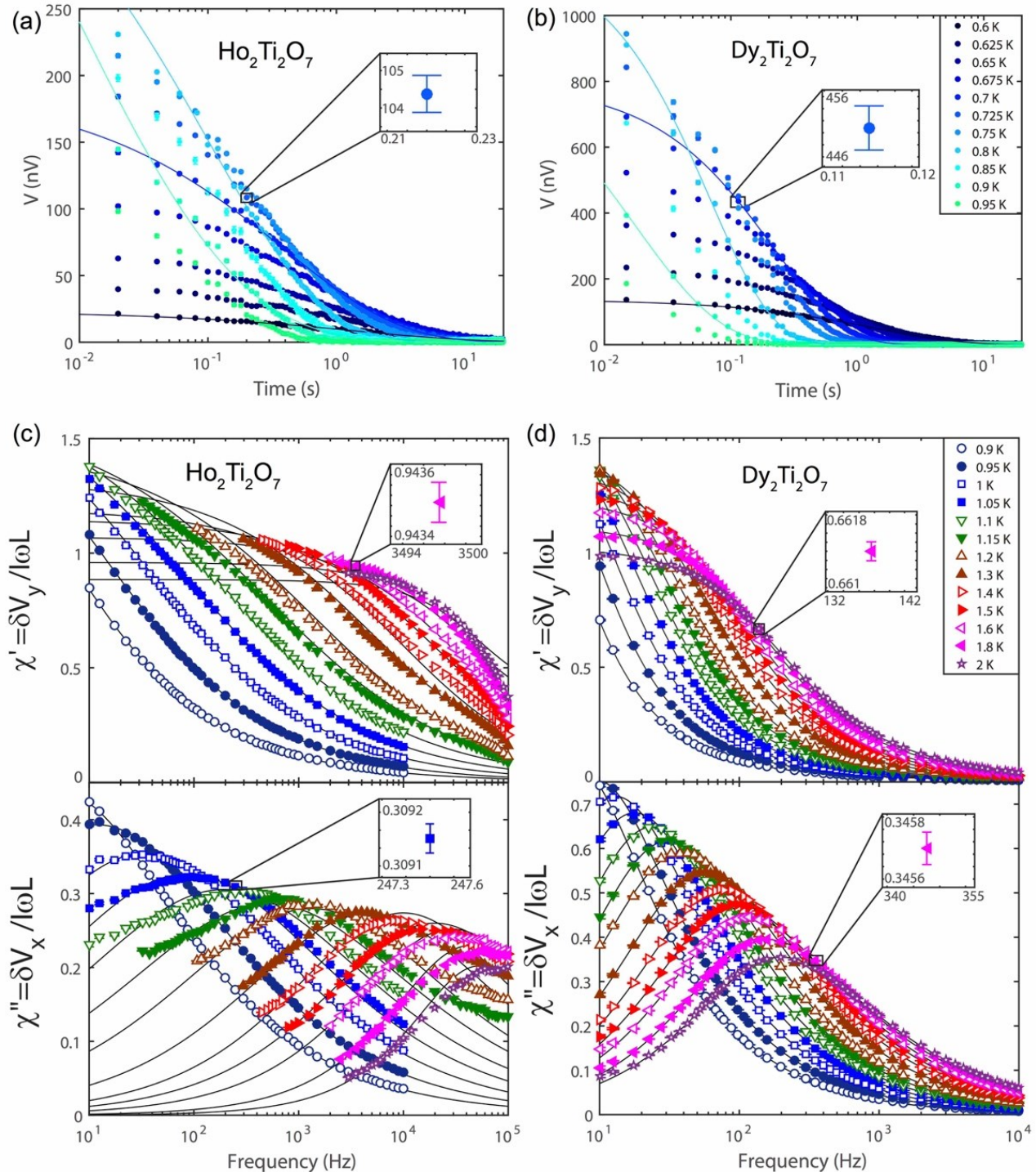


Figure 2

Comparison of the measured DC voltage and AC susceptibilities of the two lanthanide titanate pyrochlore materials, at various temperatures.

(a) and (b): Time domain magnetization relaxation measurements. At every temperature, the EMF across the STS is measured immediately after a step function change in the azimuthal magnetic field. This EMF is a measure of the magnetization change with time, $d\mathbf{M}/dt$, in $\text{Ho}_2\text{Ti}_2\text{O}_7$ (a) and $\text{Dy}_2\text{Ti}_2\text{O}_7$ (b). Fine colored curves show the fit to the KWW functional form for $V(t)$ at several representative temperatures for both materials. Insets show highly typical error bar scale for all of these EMF measurements. In both (a) and (b) the error bars are generally smaller than the points used to represent data values.

(c) Measured real (top panel) and imaginary (bottom panel) parts of the $\chi(\omega, T)$ of $\text{Ho}_2\text{Ti}_2\text{O}_7$ and (d) $\text{Dy}_2\text{Ti}_2\text{O}_7$. The AC susceptibility was calculated from the four-probe measurement of the self-inductance of STS according to equation (5) in the text. Fine black lines associated with each set of symbols representing measured $\chi(\omega, T)$ at a given T , are the Havriliak-Negami form of $\chi(\omega, T)$ fitted to $\chi'(\omega, T)$ and $\chi''(\omega, T)$ at that T . Insets show highly typical error bar scale for all of these $\chi'(\omega, T)$; $\chi''(\omega, T)$ measurements. In both (c) and (d) all error bars are shown but are generally much smaller than the points used to represent data values.

Figure 3

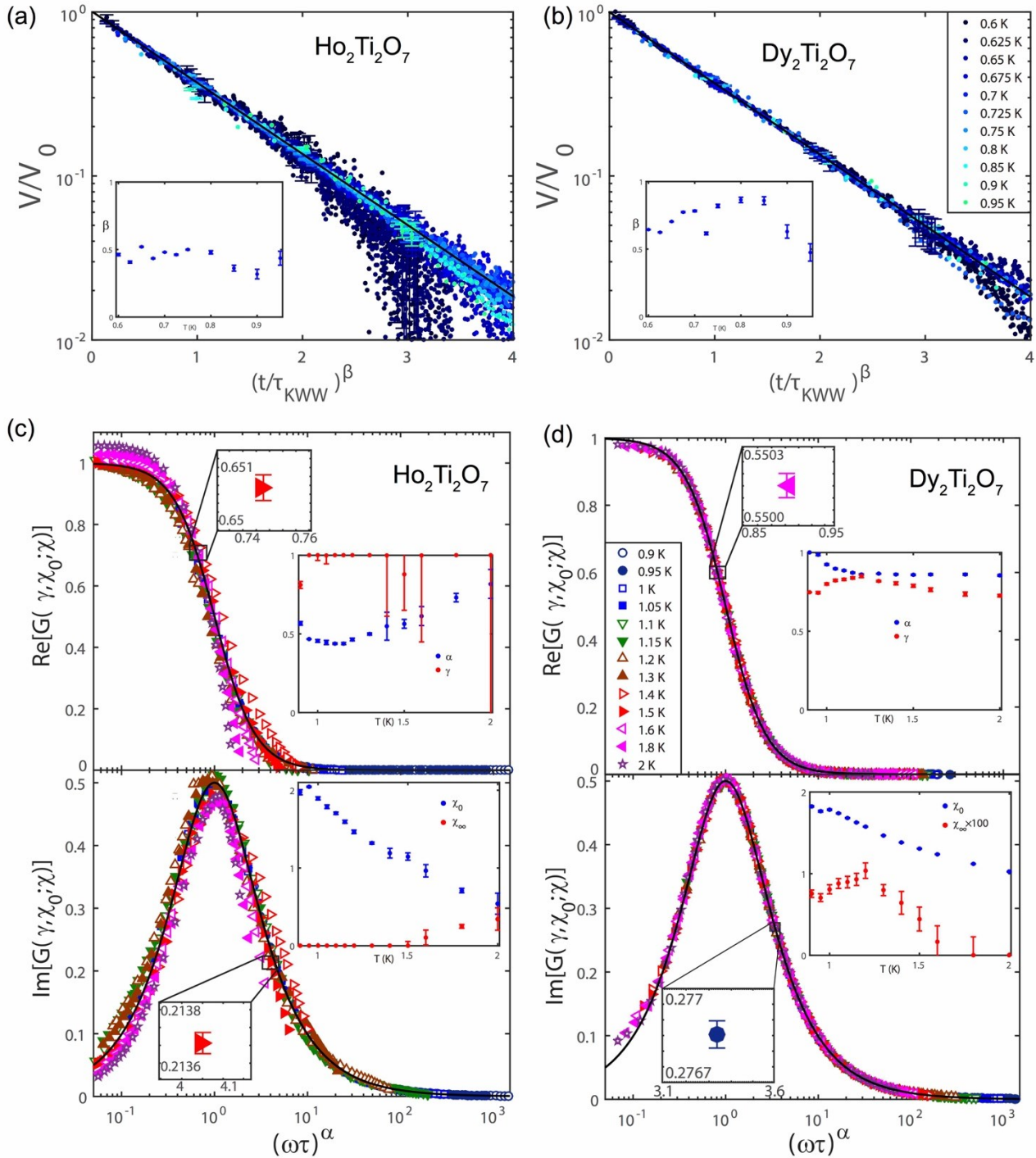


Figure 3

Comparison between $\text{Ho}_2\text{Ti}_2\text{O}_7$ and $\text{Dy}_2\text{Ti}_2\text{O}_7$ of the collapsed data sets of both DC and AC susceptibility at all measured temperatures, using the fit parameters from fitting the data to the KWW and HN forms (see text and Fig. 2c,d).

(a) and (b) The horizontal axis is modified to account for the temperature dependence of the fit parameters of the time domain magnetization relaxation measurement, $\beta(T)$ and $\tau(T)$ for (a) $\text{Ho}_2\text{Ti}_2\text{O}_7$ and (b) $\text{Dy}_2\text{Ti}_2\text{O}_7$. The vertical axis is modified from raw data by dividing by the fit parameter V_0 of the KWW form, $V(t) = V_0 \exp(-\left(\frac{t}{\tau}\right)^\beta)$. The collapse of the data for both $\text{Ho}_2\text{Ti}_2\text{O}_7$ and $\text{Dy}_2\text{Ti}_2\text{O}_7$ onto a single straight line shows a universal KWW form for all temperatures measured. Insets: temperature dependence of the exponent β for $\text{Ho}_2\text{Ti}_2\text{O}_7$ (a) and for $\text{Dy}_2\text{Ti}_2\text{O}_7$ (b). Representative error bars are shown at $x=0,1,2$ and 3 for both materials; they are difficult to see given the scatter of all the data points in the comprehensive data collapse.

(c) and (d): The real and imaginary parts of $\chi(\omega, T)$ for both $\text{Ho}_2\text{Ti}_2\text{O}_7$ and $\text{Dy}_2\text{Ti}_2\text{O}_7$, and the frequency, have been rescaled to account for the temperature dependence of all of the fit parameters in the HN form. The resulting scaled universal susceptibility function $G(\gamma, \chi_0, \chi)$ (see text and ref. 29) for (c) $\text{Ho}_2\text{Ti}_2\text{O}_7$ and (d) $\text{Dy}_2\text{Ti}_2\text{O}_7$ from all ω and T converges onto a single curve for both materials. This universal form for $\chi(\omega, T)$ is shown using the overlaid fine black curves, and obviously accurately depict $\chi(\omega, T)$ for all ω and T for both materials. Insets: temperature dependence of the HN exponents, α and γ , for $\text{Ho}_2\text{Ti}_2\text{O}_7$ and $\text{Dy}_2\text{Ti}_2\text{O}_7$ (top panel of (c) and (d) respectively), and the temperature dependence of the coefficients, χ_0 and χ_∞ , for both materials (bottom panel of (c) and (d) respectively). Small insets show highly typical error bar magnitude for all of these scaled data.

Figure 4

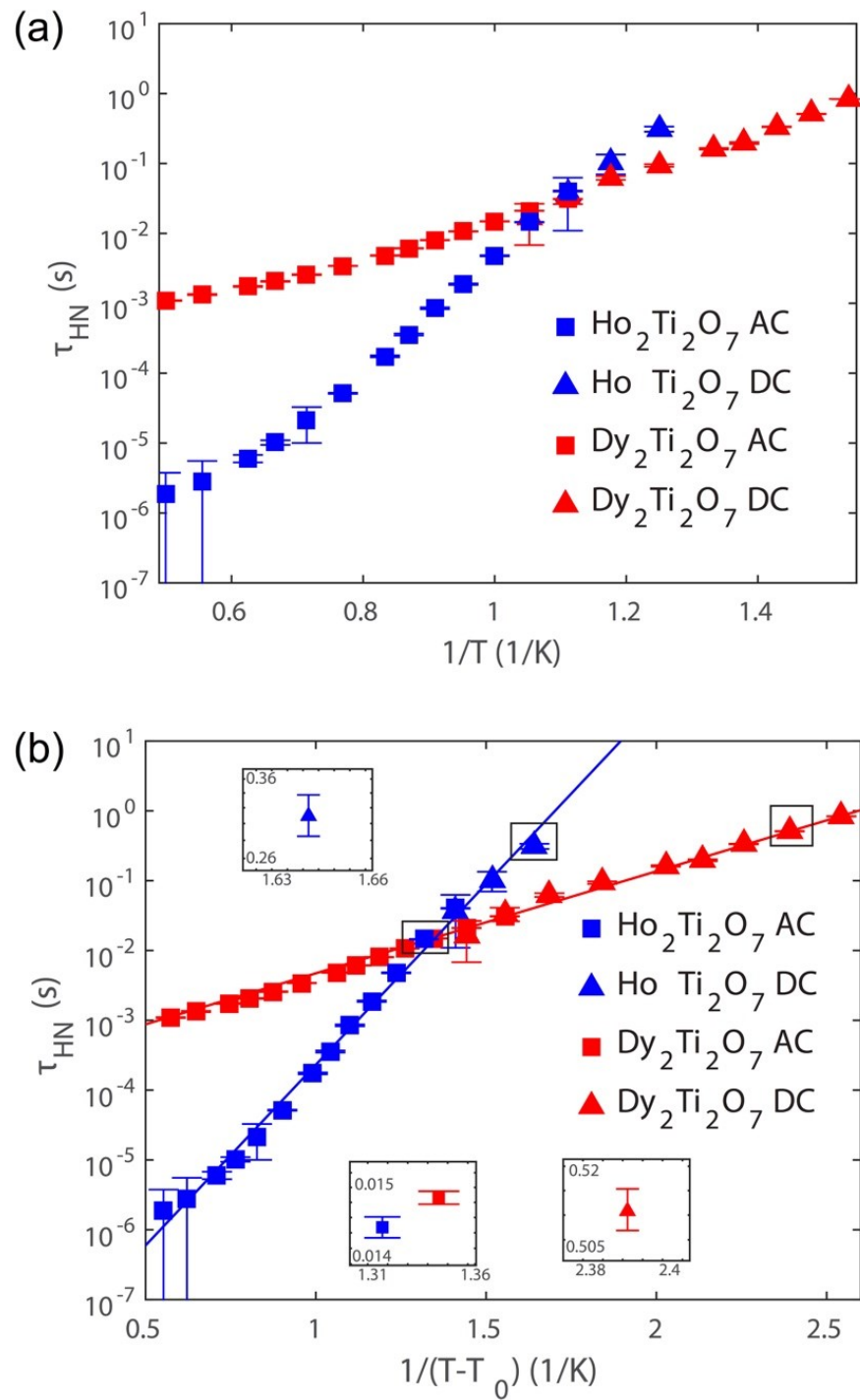


Figure 4

(a) Temperature dependence of the relaxation times obtained from the frequency (AC shown as triangles) and time (DC shown as squares) domain measurements for both $\text{Ho}_2\text{Ti}_2\text{O}_7$ and $\text{Dy}_2\text{Ti}_2\text{O}_7$. In the region where the AC and DC determined relaxation times overlap, they obviously merge smoothly. (b) A super-Arrhenius VTF function of the form $\tau(T) = A \exp\left(\frac{DT_0}{T-T_0}\right)$ fits the temperature dependence of the relaxation times yielding a divergence around $T_0 \approx 200\text{mK}$ for both materials. The fragility indices, D , however, are quite different, with $\text{Dy}_2\text{Ti}_2\text{O}_7$ having a more fragile, $D \approx 13$, hence heterogeneous, dynamics, as expected by the more efficient tunneling of monopoles in $\text{Ho}_2\text{Ti}_2\text{O}_7$ for which $D \approx 62$ from the fit.

REFERENCES

- 1 Farmer, J. M. *et al.*, Structural and crystal chemical properties of rare-earth titanate pyrochlores, *J. Alloys and Compounds* **605**, 63 (2014).
- 2 Gardner, J. S., Gingras, M. J. P. and Greedan J. E., Magnetic pyrochlore oxides, *Rev. Mod. Phys.* **82**, 53 (2010).
- 3 Lacroix, C., Mendels, P. and Mila, F. (2011) Introduction to Frustrated Magnetism, Berlin: Springer-Verlag GmbH
- 4 Castelnovo, C., Moessner, R. and Sondhi, S., Magnetic monopoles in spin ice. *Nature* **451**, 42 (2008).
- 5 Ramirez, A. P., Hayashi, A., Cava, R. J., Siddharthan, R. and Shastry, B. S., Zero-point entropy in 'spin ice', *Nature* **399**, 333 (1999).
- 6 Snyder, J., Slusky, J. S., Cava, R. J. and Schiffer P., How 'spin ice' freezes, *Nature* **413**, 48 (2001).
- 7 Rau, J. G. and Gingras M. J. P., Spin slush in an extended spin ice model, *Nat. Comm.*, **7**, 12234 (2016).
- 8 Balents, L., Spin liquids in frustrated magnets, *Nature* **464**, 199 (2010).
- 9 Lau, G. C. *et al.*, Zero-point entropy in stuffed spin-ice, *Nature Physics* **2**, 249 (2006).
- 10 Petrenko, O. A., Lees, M. R., and Balakrishnan, G., Magnetization process in the spin-ice compound Ho₂Ti₂O₇, *Phys. Rev. B* **68**, 012406 (2003).
- 11 Rosenkranz, S. , Ramirez, A. P., Hayashi, A., Cava, R. J., Siddharthan, R. and Shastry, B. S., Crystal-field interaction in the pyrochlore magnet Ho₂Ti₂O₇, *J. Appl. Phys.* **87**, 5914 (2000).
- 12 Jana, Y. M., Sengupta, A. and Ghosh, D., Estimation of single ion anisotropy in pyrochlore Dy₂Ti₂O₇, a geometrically frustrated system, using crystal field theory, *J. Mag. Mag. Mat.* **248**, 7 (2002).
- 13 Harris, M. J., Bramwell, S. T., McMorrow, D. F., Zeiske, T. and Godfrey K. W., Geometrical Frustration in the Ferromagnetic Pyrochlore Ho₂Ti₂O₇, *Phys. Rev. Lett.* **79**, 2554 (1997).
- 14 Melko, R. G., den Hertog, B. C. and Gingras, M. J. P., Long-Range Order at Low Temperatures in Dipolar Spin Ice, *Phys. Rev. Lett.* **87**, 067203 (2001).
- 15 Fukazawa H., Melko, R. G., Higashinaka, R., Maeno, Y. and Gingras M. J. P., Magnetic anisotropy of the spin-ice compound Dy₂Ti₂O₇, *Phys. Rev. B* **65**, 054410 (2002).

16 den Hertog, B. C. and Gingras, M. J. P., Dipolar Interactions and Origin of Spin Ice in Ising Pyrochlore Magnets, *Phys. Rev. Lett.* **84**, 3430 (2000).

17 Jaubert, L. D. C. and Holdsworth, P. C. W., Magnetic monopole dynamics in spin ice, *J. Phys: Cond. Mat.* **23**, 164222 (2011).

18 Lummen, T. T. A., *et al.*, Phonon and crystal field excitations in geometrically frustrated rare earth titanates, *Phys. Rev. B* **77**, 214310 (2008).

19 Tomasello, B., Castelnovo, C., Moessner, R. and Quintanilla, J., Single-ion anisotropy and magnetic field response in the spin-ice materials Ho₂Ti₂O₇ and Dy₂Ti₂O₇, *Phys. Rev. B* **92**, 155120 (2015).

20 Bramwell, S. T. *et al.*, Spin Correlations in Ho₂Ti₂O₇: A Dipolar Spin Ice System, *Phys. Rev. Lett.* **87**, 047205 (2001).

21 Van Kempen, H., Miedema, A. R. and Huiskamp, W. J., Heat capacities of the metals terbium and holmium below 1°K, *Physica* **30**, 229 (1964).

22 Fennel, T., Bramwell, S. T., McMorrow, D. F., Manuel, P. and Wildes, A. R., Pinch points and Kasteleyn transitions in kagome ice, *Nat. Phys.* **3**, 566 (2007).

23 Fennell, T. *et al.*, Magnetic Coulomb Phase in the Spin Ice Ho₂Ti₂O₇, *Science* **326**, 415 (2009).

24 Yavors'kii, T., Fennell, T., Gingras, M. J. P. and Bramwell, S. T., Dy₂Ti₂O₇ Spin Ice: A Test Case for Emergent Clusters in a Frustrated Magnet, *Phys. Rev. Lett.* **101**, 037204 (2008).

25 Takatsu, H. *et al.*, AC Susceptibility of the Dipolar Spin Ice Dy₂Ti₂O₇: Experiments and Monte Carlo Simulations, *J. Phys. Soc. Jpn.* **82**, 104710 (2013).

26 Ryzhkin, I. A., Magnetic relaxation in rare-earth oxide pyrochlores, *J. Expt. Theo. Phys.* **101**, 481 (2005).

27 Jaubert L. D. C. and Holdsworth, P. C. W., Signature of magnetic monopole and Dirac string dynamics in spin ice, *Nat. Phys.* **5**, 258 (2009).

28 Yaraskevitch, L. R. *et al.*, Spin dynamics in the frozen state of the dipolar spin ice material Dy₂Ti₂O₇, *Phys. Rev. B* **85**, 020410 (2012).

29 Kassner, E.R., Eyvazov, A. B., Pichler, B., Munsie, T. J. S., Dabkowska, H. A., Luke, G. M. and Davis, J. C. S., *PNAS* **112**, 8549 (2015).

30 Ediger, M., Angell, C. and Nagel, S., Supercooled Liquids and Glasses. *J. Phys. Chem.* **100**, 13200 (1996).

31 Tarjus, G., Kivelson, S., Nussinov, Z. and Viot, P., The frustration-based approach of supercooled liquids and the glass transition: a review and critical assessment. *J. Phys.: Condens. Matt.* **17**, R1143 (2005).

32 Cavagna, A., Supercooled liquids for pedestrians. *Physics Reports* **476**, 51 (2009).

33 de Souza, V. K. and Wales, D. J., Correlation effects and super-Arrhenius diffusion in binary Lennard-Jones mixtures, *PHYS. REV. B* **74**, 134202 (2006).

34 Bohmer, R., Ngai, K., Angell, C. and Plazek, D., Nonexponential relaxations in strong and fragile glass formers. *J. Chem. Phys.* **99**, 4201 (1993).

35 Havriliak, S. and Negami, S., A Complex Plane Representation of Dielectric and Mechanical Relaxation Processes in Some Polymers. *Polymer* **8**, 161 (1967).

36 Havriliak, Jr. S. and Havriliak, S., Results from an unbiased analysis of nearly 1000 sets of relaxation data. *J. Non-Cryst. Solids* **172**, 297 (1994).

37 Kohlrausch, R., Theorie des elektrischen ruckstandes in der leidner flasche. *Annelen der Physik und Chemie (Poggendorff)* **91**, 179 (1854).

38 Ediger, M. D., Spatially heterogeneous dynamics in supercooled liquids, *Ann. Rev. Phys. Chem. b*, **99** (2000).

39 Ehlers, G., Cornelius, A. L., Orendac, M. , Kajnakova, M., Fennell, T., Bramwell, S. T. and Gardner, J. S., Dynamical crossover in 'hot' spin ice, *J. Phys.: Condens. Matter* **15** (2003).

40 Rau, J. G. and Gingras, M. J. P., Magnitude of quantum effects in classical spin ices, *Phys. Rev. B* **92**, 144417 (2015).

41 Alvarez, F., Alegria, A. and Colmenero, J., Relationship between the time-domain Kohlrausch-Williams-Watts and frequency-domain Havriliak-Negami relaxation functions, *Phys. Rev. B* **44**, 7306 (1991).

42 Snyder, J. *et al.*, Low-temperature spin freezing in the Dy₂Ti₂O₇ spin ice, *Phys. Rev. B* **69**, 064414 (2004).

43 Quilliam, J. A., Yaraskavitch, L. R., Dabkowska, H. A., Gaulin, B. D. and Kycia, J. B., Dynamics of the magnetic susceptibility deep in the Coulomb phase of the dipolar spin ice material Ho₂Ti₂O₇, *Phys. Rev. B* **83**, 094424 (2011).

44 Matsuhira, K., Hinatsu, Y. and Sakakibara, T., Novel dynamical magnetic properties in the spin ice compound Dy₂Ti₂O₇, *J. of Phys.: Condensed Matter* **13**, 31 (2001).

45 Castelnovo, C., Moessner, R. and Sondhi, S., Debye-Hückel theory for spin ice at low temperature, *Phys. Rev. B* **84**, 144435 (2011).

46 Udagawa, M., Jaubert, L. D. C., Castelnovo, C. and Moessner R., Out-of-equilibrium dynamics and extended textures of topological defects in spin ice, *Phys. Rev. B* **94**, 104416 (2016).

47 Dąbkowska, H.A., Dąbkowski, A.B., Hermann, R., Priede, J. and Gerbet, G. (2015) Floating Zone Growth of Oxides and Metallic Alloys. pp. 281–329 In: Nishinaga, T. and Rudolph, P., *Handbook of Crystal Growth*, Vol. II. Elsevier, B.V.